SAND2015-2424C

ILASS Americas 27th Annual Conference on Liquid Atomization and Spray Systems, Raleigh, NC, May 2015

Characterization of drop aerodynamic fragmentation in the bag and shear thinning regimes by crossed-beam two-view digital in-line holography

Jian Gao[a], Daniel R. Guildenbecher[*,b], Kathryn N. Gabet-Hoffmeister[b], Jun Chen[c], and Paul E. Sojka[c]
[a]Laboratory for Experimental Fluid Dynamics, Johns Hopkins University, Baltimore, MD, USA
[b]Sandia National Laboratories, Albuquerque, NM, USA
[c]School of Mechanical Engineering, Purdue University, West Lafayette, IN, USA

Abstract

In our 2014 ILASS-Americas presentation we proposed a cross-beam, two-view digital in-line holography (DIH) configuration to quantify the size and velocity of fragments which are generated by the breakup of an ethanol drop in an air stream. There it was shown that the cross-beam configuration overcomes the depth of focus challenges in DIH and allows for accurate quantification of fragment size probability density functions, *pdf*(*d*), and size-velocity correlations. Here, the technique is applied to study the spatial and temporal evolution of these quantities for drops undergoing breakup in the bag and sheet thinning regimes. Reconstructed holograms quantitatively illustrate how drop and fragment position, morphology, size, and velocity vary with spatial position and time. In particular, the existence of a second peak in *pdf*(*d*) is shown to arise due to rim fragmentation in the bag breakup regime ($We = 14$). In addition, the velocities of the fragments show little correlation with size. In contrast, *pdf(d)* is always mono-modal for the sheet thinning case, likely due to the continuous breakup of the original drop core. In that case, the velocities of the smaller drops appear to exceed that of the larger drops. Finally, results show that the temporal behaviors of D_{10}, D_{30}, D_{32} and MMD, as well as the ratio of MMD/D_{32}, can be dependent on time and *We*.

[*]Corresponding author: drguild@sandia.gov

Introduction

It is well known that a liquid drop moving through a surrounding gas with non-zero velocity will experience some form of deformation. This is due to the competition between aerodynamic drag, which applies a non-uniform force to the drop surface, and interfacial tension, which attempts to counteract that force distribution with a consolidating force. If the former is sufficiently greater than the latter the drop may be deformed to the point of fragmentation. This is referred to as secondary breakup [1].

Secondary breakup, as illustrated in Figure 1 from [2], has become something of a canonical flow problem due to its presence in many practical sprays, its inclusion of interfacial as well as internal and external flow physics, and an initial geometry that lends itself to experimental, analytical and computational investigation. As such, it has been studied for decades.

Early experimental work, most notably by Faeth and colleagues [3-8] plus Reitz and coworkers [9-13], focused on identifying breakup process morphologies and flow conditions for inter-regime boundaries (typically in terms of Weber number, $We = \rho_g d_0 u_0^2/\sigma$, but also in terms of Ohnesorge number when viscous effects are important). More than ten years of work led to the general agreement that there are five separate modes of breakup: vibrational, bag, bag-and-stamen (sometimes called multi-mode), sheet-thinning (previously termed shear stripping), and catastrophic. These authors also provided phenomenological guidelines for some drop size distribution characteristic diameters ($MMD/D_{32} \sim 1.2$) and suggestions as to appropriate drop size distribution functions. Little was mentioned regarding the distribution of fragment velocities.

More recent work by Theofanous *et al*. [14-16] has taken a different approach. They argue that drop fragmentation is due to Rayleigh-Taylor piercing at lower *We* and shear-induced entrainment above a transition *We*. The controversy between the Faeth and coworkers and Reitz and colleagues work with that of Theofanous *et al*. has yet to be resolved.

Early analytical work (the TAB model of [17, 18], and perhaps as far back as GI Taylor [19, 20] and Lamb [21]) used force or energy concepts to derive simplified models for drop deformation. Later work by Sellens and Brzustowski [22] and Li and Tankin [23] employed Shannon-like entropy maximization approaches to derive joint size-velocity pdfs. Comparisons were made between model predictions and experimental data. Identified limitations were the use of *ad hoc* constraints or physical sub-models, some of which were of debatable merit.

This approach has been shown to have limitations though. Van der Geld and Vermeer [24] showed that the Shannon entropy should not be used if drop volume is used instead of diameter. Dumochel and coworkers [25-27] first rigorously developed the appropriate formalism, showing that the number *pdf* should be predicted unless the additional information of spherical drops is incorporated, then included non-equal probability for drop size classes, and suggested values for the two model parameters might be dependent on atomizer hardware. Li *et al*. [28] incorporated a series of constraints based on characteristic drop diameters, which are difficult to predict *a priori*. These and other works have been reviewed by Dechelette *et al*. [29], who concluded that constraints should be written in terms of distribution characteristic diameters (which must be determined by some other means), one constraint is not enough to provide physically sensible predictions, and at this time it appears to be impossible to predict more than one characteristic size.

Secondary breakup computational studies do not have as long a history as the corresponding experimental and analytical efforts. The first study relevant to deforming drops may be that of Masliyah and Epstein [30], who solved the Navier-Stokes equations for axisymmetric oblate and prolate spheroid flows at $Re < 100$. In the intervening years until 2015, a number of groups have considered some combination of non-isothermal, deforming, unsteady, viscous, evaporating cases. Examples include studies by Tryggvason and colleagues [31-33], Quan and co-workers [34-36], Abraham *et al*. [37, 38], and, most recently, Kekesi *et al*. [39].

Improvement and validation of all of these modeling efforts requires in-depth quantification of this transient, multiphase flow. However, previous experimental quantification has been mostly limited to imaging (such as Figure 1) for determination of flow morphologies, while a few studies have attempted to quantify fragment sizes and velocities using point-wise phase Doppler anemometery (PDPA) [40] and some analog holography [4, 5, 7, 8, 41, 42]. Nevertheless, datasets remain sparse. In our previous work [43-45] we demonstrated digital in-line holography (DIH) for characterization of fragment sizes and velocities in 3D space. Advantages of this technique include a large field of view and automatic processing routines, which allow for rapid quantification of particle statistics. Most recently, a cross-beam, two-view DIH configuration was proposed by Gao *et al.* [43]. Using two DIH views, this method overcomes the depth of focus problem discussed in [46]. Consequently, as shown in [43], the cross-beam, two-view configuration provides accurate quantification of all three velocity components and effectively filters false positives from the drop size distribution. This work continues those efforts by investigating conditions leading to bag and sheet-thinning breakup. Using the cross-beam, two-view configuration, size and velocity statistics are resolved as a function of time and space.

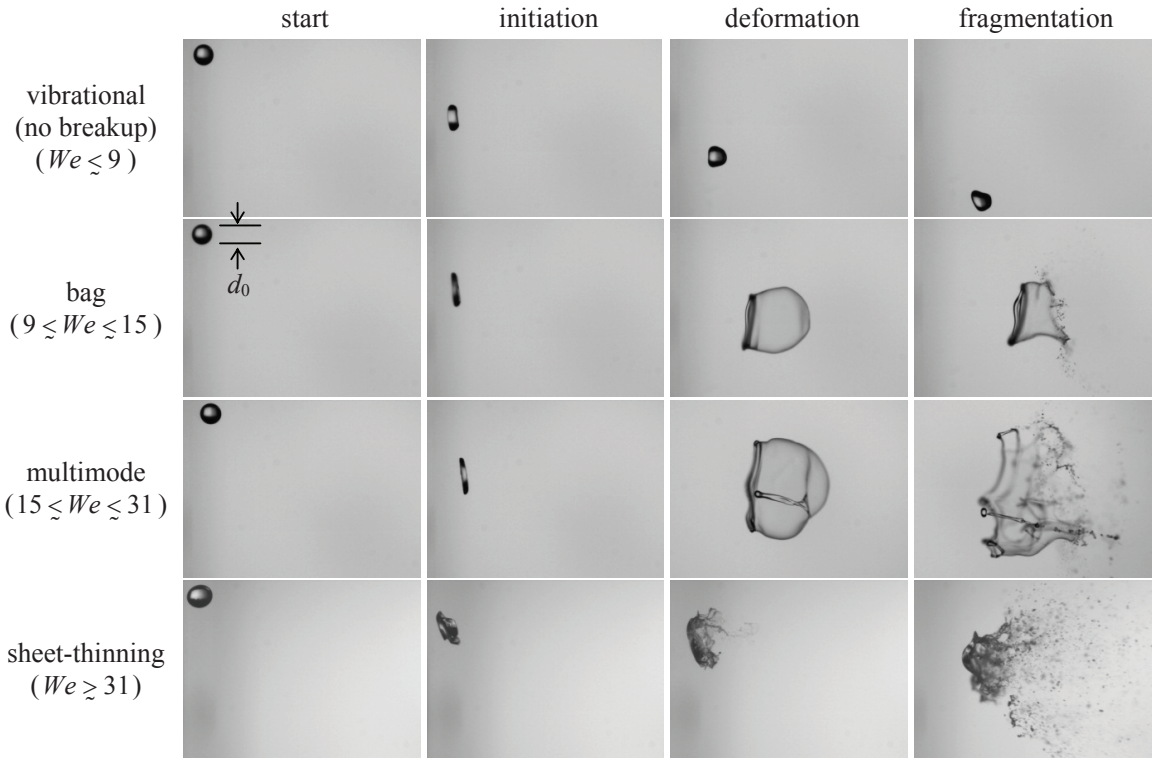

Figure 1. Shadowgraphs of ethanol drops undergoing aerodynamic fragmentation. Time increases from left to right, disruptive forces increase from top to bottom. Images are from Guildenbecher and Sojka [2] and were acquired using an experimental configuration similar to that used in the present work.

Experimental methods

The experimental apparatus is that of Gao *et al*. [43], and is shown in Figure 2. Single drops are generated by syringe pumping a liquid to a dispensing tip that is mounted above an air nozzle. Measurements are initiated when a drop falls through a laser beam and partially obstructs the signal to a photodetector. This supplies a trigger pulse to the digital cameras, which record the breakup process. All drops are formed using ethanol with assumed surface tension, $\sigma = 0.0244$ N/m.

The crossed-beam two-view DIH set up is also that of Gao *et al*. [43] and shown in Figure 3. The double-pulse output from a Nd:YAG laser is split into two beam paths which are each spatially filtered, expanded and collimated before illuminating the drop breakup process. Both beam axes lay in the *x*-*z* plane. Beam 1 axis is collinear with the *z*-axis while the beam 2 axis is rotated away from it through a small angle, $\theta = 0.335 \pm 0.002$ radians [43].

The interference patterns produced by fragmenting drops are recorded using a pair of CCD cameras (4008 × 2672 pixels, 9 μm pixel pitch) operated in double exposure mode and synchronized with the double laser pulses. The inter-fame time between laser pulses, Δt, is chosen such that particles move a few 10s of pixels between frames. For the conditions considered here Δt varies between 16 and 33.5 μs.

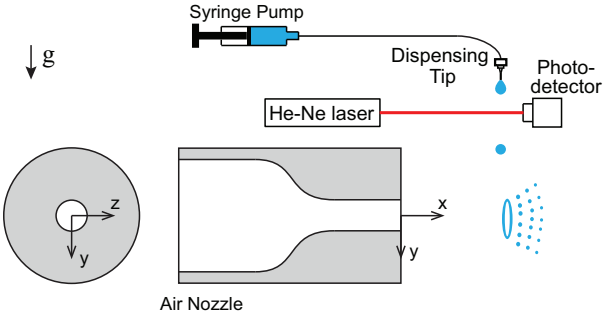

Figure 2. Gao *et al*. [43] apparatus to produce aerodynamic drop fragmentation.

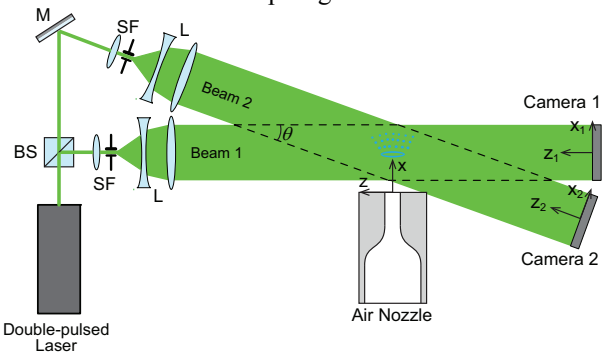

Figure 3. Gao *et al*. [43] crossed-beam, two-view DIH configuration, BS: beam splitter, M: mirror, SF: spatial filter, L: lens: θ: angle between the two beams.

The time delay between the photodetector trigger and the firing of the holography laser is adjusted to investigate different phases of the breakup process. At the same time, the field of view is translated to the appropriate downstream position using a traverse.

Figure 4 shows sample holograms from views 1 and 2 for flow conditions leading to the bag breakup morphology. Two clearly different sizes of fragments are observed. The larger ones result from rim breakup while the smaller ones are a consequence of bag breakup. Each of these holograms is initially processed using the hybrid method described in [43, 47-49] to measure the 3D coordinates and 2D morphology of all particles within the field of view. To prevent detection of small regions of noise, no particle is accepted with area equivalent diameter, $d \leq 27$ μm. Similarly, to eliminate detection of the intact core of the original drop, no region is accepted with $d \geq 2$ mm.

As described in Gao *et al* [43], 3D particle displacements are first found in each of the two fields of view by matching the measured particle positions to their neighbors in the second frame recorded Δt after the first. Here, the match probability method (Hungarian routine) of Tinevez [50] is utilized. No match is accepted when the total *x*-*y*-*z* displacement is greater than 1 mm. The top row in Figure 5(a) shows the measured in-plane (*x*-*y*) sizes and velocities from view 1 while the bottom row shows the out-of-plane, (*x*-*z*) velocities. From these results is it clear that the single view DIH produces reasonable estimates of the in-plane sizes and velocities. However, out-of-plane velocities appear to contain many erroneous vectors. This can be attributed to the high depth-uncertainty in DIH discussed in [46].

To improve upon this, Gao *et al*. [43] proposed the two-view configuration. After spatially calibrating view 2 to view 1, particle positions measured in view 2 are transformed to the view 1 coordinate system. Next, matching is performed to pair individual particles measured in both views. This is used to eliminate potentially erroneous particles whose diameter varies by more than 15% between the two views. For the remaining particles, the out-of-plane, Δz, displacement is found by

$$\Delta z = \cot\theta \Delta x_1 - \Delta x_2 / \sin\theta , \qquad (1)$$

where Δx_1 is the *x*-displacement measured over Δt in view 1 and Δx_2 is the *x*-displacement measured in view 2. Note, Eq. (1) does not directly depend on the measured *z*-displacements in either view. Consequently, the measured out-of-plane velocity is significantly more accurate. This is illustrated in Figure 5(b) which shows the in-plane (*x*-*y*) sizes and velocities (top) and out-of-plane (*x*-*z*) velocities (bottom) measured after performing the two-view matching. Compared to Figure 5(a) the particle *x*-*z* velocities appear to more closely match the expected flow symmetry with dispersion of the particles away from the center of breakup.

The dual-view method causes some reduction in the total number of drops measured, but does a good job of eliminating erroneous particle sizes which occur when two closely spaced particles are measured as a single particle in one view (for example, see the large region in the lower left circled in red in the top image of Figure 5(a)). The method also greatly improves the out-of-plane velocity accuracy [43]. Further details, including quantification of measurement uncertainty, are provided in Gao *et al*. [43].

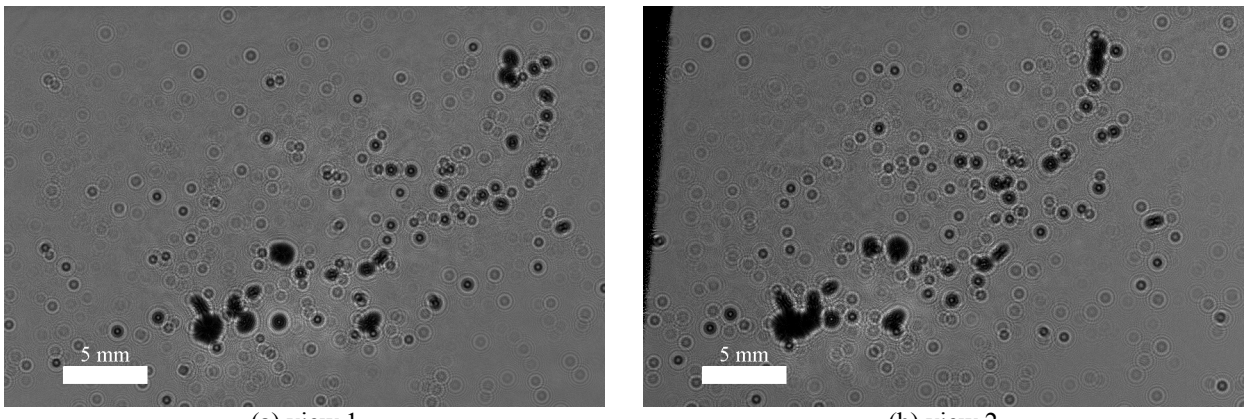

(a) view 1 (b) view 2

Figure 4. Sample holograms at *We* = 14, showing diffraction pattern due to larger fragments from rim breakup and smaller fragments from breakup of the bag (also see Figure 6e).

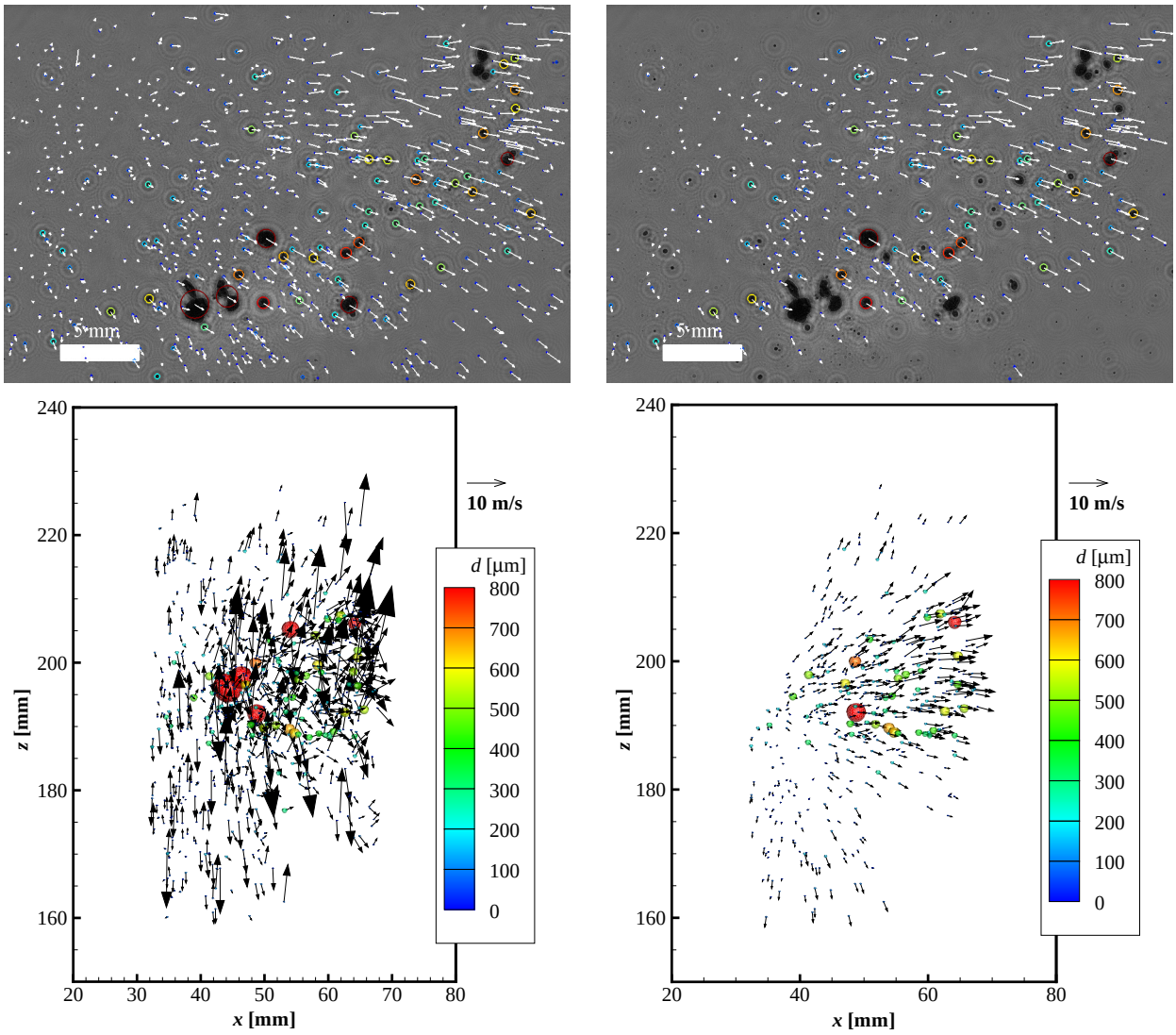

Figure 5. (Top) Size and *x*-*y* velocities measured in the hologram plane and (bottom) *x*-*z* velocities measured in the out-of-plane direction from (a) single beam (view 1) DIH and (b) the crossed-beam two-view DIH configuration.

Results

In this section, results are presented for two flow conditions corresponding to the bag breakup and sheet thinning regimes. In all cases, the drops leave the syringe tip with approximately zero velocity and fall 174 ± 5 mm before reaching the centerline of the air nozzle. Table 1 summarizes the other initial conditions. Here, the initial drop diameter, d_0, and *x*-location where the drop is injected into the air flow, x_0, are measured from 20 holograms recorded of the initial drop without the air flow. For those parameters, the reported uncertainty is the standard deviation of the measured quantities. The initial centerline air velocity u_0, is estimated from previous measurements of this flow [51, 52]. The reported uncertainty is the root mean square of the flow fluctuations measured in [51]. Finally, the *We* is found assuming constant air density $\rho_g = 1.2$ kg/m^3, with uncertainty estimated by propagation of measured uncertainties.

Table 1. Initial conditions for the two breakup morphologies.

Morphology	Initial *x*-location, x_0 [mm]	Initial drop diameter, d_0 [mm]	Air mass flow rate [kg/min]	Centerline air velocity, u_0, at the initial *x*-location [m/s]	Weber number, *We*
Bag	8.8 ± 0.1	2.54 ± 0.02	0.35	10.5 ± 0.2	13.8 ± 0.5
Sheet-thinning	8.9 ± 0.2	2.55 ± 0.01	0.70	21.0 ± 0.5	55.3 ± 2.6

Figure 6 and Figure 7 show bag and sheet thinning fragmentation, respectively, along with the size probability density function, *pdf*(*d*), and size-velocity correlation. In each case *pdf*(*d*) is the number *pdf* of all particles measured from 44 realizations at each field of view. The size-velocity correlations are also built from all data. Finally, the reported time is with respect to the first image shown. Several important conclusions can be drawn.

For bag breakup (at *We* = 14), Figure 6 data show:

1) The *pdf*(*d*) evolves from a mono-modal form at times less than 25 ms (i.e., prior to rim breakup) to a bi-modal form as rim fragmentation progresses to completion (Note the secondary peak around 500 μm in Figure 6(f).) The rise of this second peak in the *pdf*(*d*) as the rim fragments suggests that classical mono-modal drop size distribution models (such as root-normal, log-normal, Rosin-Rammler, Nukiyama-Tanasawa, etc.) will be inaccurate during that time.
2) The velocity data exhibit the expected decline in mean velocity with time (due to diminishing aerodynamic drag and decreased mean jet velocities at increasing *x*). However, the size-velocity data show no clear correlation. Typically, a negative size velocity correlation is expected as smaller drops are accelerated more quickly by the gas flow compared to larger drops. Here, it is possible that at late time, gravity has accelerated most of the drops out of the main flow region of the air jet. This non-ideal boundary conditions is a limitation of the current experimental configuration. Still, the dimensions of the air nozzle are well documented and the initial trajectory and drop deformation is also well characterized by Flock *et al*. [52]. Therefore, this data set is well-suited for validation of computational models.

For sheet-stripping breakup (*We* = 55), Figure 7 data show:

1) The *pdf*(*d*) retains its mono-modal form throughout the fragmentation process. This is expected since there is no rim breakup process that would lead to a second population of larger fragments. Note that the observed increase in the tail at large diameters is due to continual breakup of the original drop core.
2) The size-velocity data show some correlation in this case, with the largest fragments traveling slowest. This is to be expected because the small fragments are formed by stripping mass from the drop perimeter, giving them a larger velocity than the original drop core and its subsequent fragments. This size-velocity correlation diminishes at longer times as the original drop core accelerates such that its fragments are moving at speeds closer to those of the small fragments formed during stripping.

Figure 8 presents are more macroscopic view by showing the evolution of some commonly reported characteristic diameters. Note that Figure 8 includes additional results for some delay time/positions in between those shown in Figure 6 and Figure 7. Interesting findings include:

1) The higher *We* case actually produces larger drops at earlier times. This is probably because the sheet-thinning mechanism produces larger fragments compared to those resulting from rupture of the thin bag.
2) In contrast, the lower *We* case shows larger characteristic diameters at later times, especially D_{32} and MMD. This is probably due to ring collapse, which produces a number of very large fragments all having approximately the same size.

Figure 9 shows the ratio of mass median diameter to Sauter mean diameter, MMD/D_{32}, as a function of time. Previous work indicates that aerodynamic driven spray formation processes generally lead to fragments having $MMD/D_{32} \approx 1.2$ [53]. The dotted line in Figure 9 illustrates this relation, while the symbols are from our experimental results. The figure shows that at early times both bag and sheet-thinning data agree with this relation to within the experimental uncertainty. However, at late times MMD/D_{32} calculated from bag data visibly exceeds 1.2, probably due to ring breakup.

Summary and Conclusions

In the current study cross-beam, two-view digital in-line holography (DIH) is applied to acquire 3D fragment positions, size-velocity correlations, fragment size probability density functions, *pdf*(*d*), and fragment morphologies for drops undergoing bag and sheet thinning breakup. The reconstructed holograms quantitatively illustrate how drop and fragment position, morphology, size, and velocity vary with spatial position (and time), in particular:

- For bag breakup, the size probability density function, *pdf*(*d*), evolves from a mono-modal form prior to rim breakup to a bi-modal form after rim breakup.
- No significant size-velocity correlation is observed for fragments formed during bag breakup. This may be due to limitations of the current configuration which lead to drops leaving the main gas flow at late times.
- For sheet-thinning breakup, *pdf*(*d*) remains mono-modal over time. This is probably because breakup of the original drop core occurs randomly in time and produces randomly sized fragments
- There is evidence of a size-velocity correlation for fragments formed via sheet-thinning breakup, with larger drops moving more slowly than smaller drops.

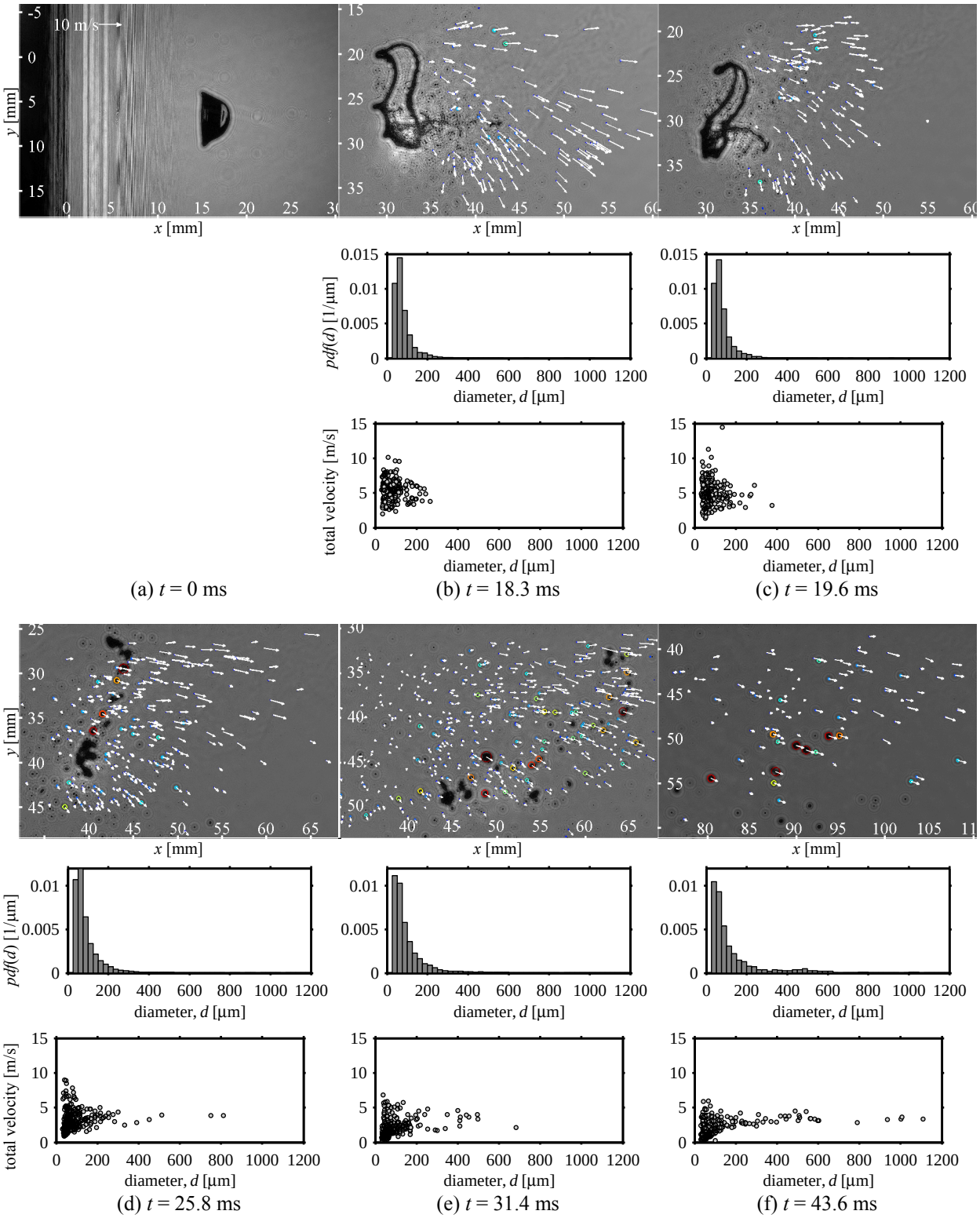

(a) $t = 0$ ms (b) $t = 18.3$ ms (c) $t = 19.6$ ms

(d) $t = 25.8$ ms (e) $t = 31.4$ ms (f) $t = 43.6$ ms

Figure 6. Selected DIH results for $We = 13.8 \pm 0.5$. All images are of the view 1 hologram refocused to the mean z location, then overlaid with the in-plane velocities and sizes measured from the dual-view configuration (see Figure 5 for size color scale; all times are relative to that of the first image). The number probability density function, $pdf(d)$, is calculated from 44 realizations at each initial condition. Finally, size-velocity maps are built from all realizations (250 data points shown, selected at random from all measured particles).

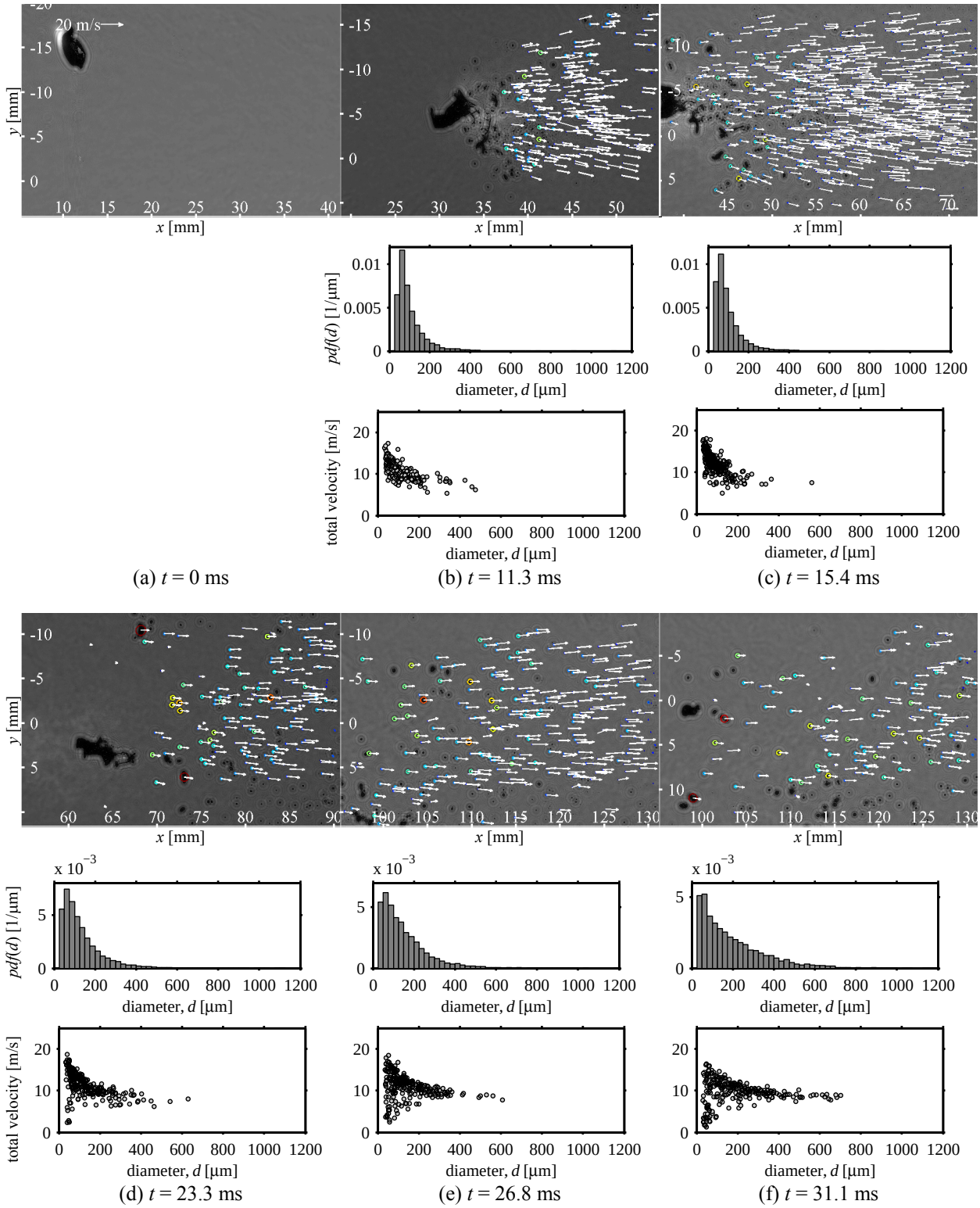

Figure 7. Selected DIH results for $We = 55.3 \pm 2.6$. All images are of the view 1 hologram refocused to the mean z location, then overlaid with the in-plane velocities and sizes measured from the dual-view configuration (see Figure 5 for size color scale; all times are relative to that of the first image). The number probability density function, $pdf(d)$, is calculated from 44 realizations at each initial condition. Finally, size-velocity maps are built from all realizations (250 data points shown, selected at random from all measured particles).

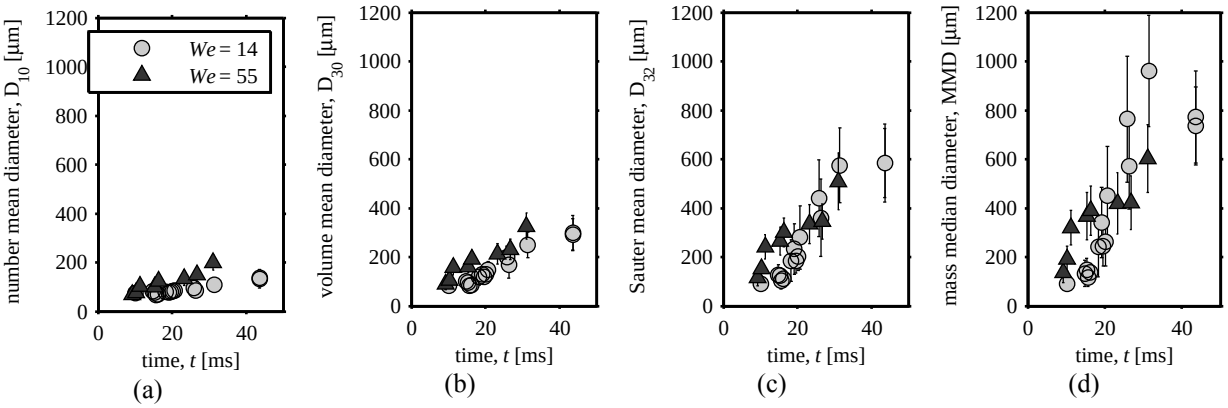

Figure 8. Evolution of characteristic mean drop sizes: (a) number mean diameter, D_{10}, (b) volume mean diameter, D_{30}, (c) Sauter mean diameter, D_{32}, and (d) mass median diameter, MMD.

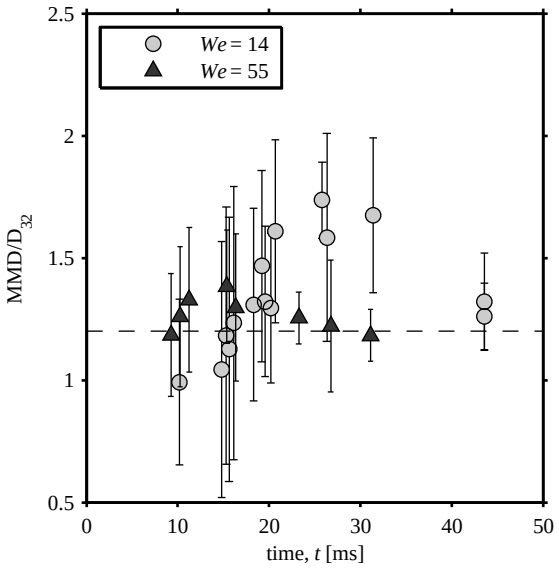

Figure 9. Ratio of mass median diameter (MMD) to Sauter mean diameter (D_{32}) versus time.

- The sheet-thinning case produces larger fragments at earlier times in comparison to bag breakup. This is most likely due to very small fragments being formed from the thin walled bag.
- The bag breakup case produces larger fragments at later times due to rim collapse into larger sub-units. These larger sub-units are less likely to undergo further breakup than their sheet-thinning counterparts because their *We* magnitudes are too low to induce further disintegration.
- Temporal behavior of the ratio MMD/D_{32} is seen to always be within experimental uncertainty of Simmons' [53] value of 1.2 for sheet-thinning breakup, but not for bag breakup. In the latter case the experimentally determined ratio was within experimental uncertainty only until rim breakup occurred.

Several key conclusions can be drawn from the results presented here:

- A universal functional form for fragment size distribution does not exist if drops are undergoing bag and sheet-thinning breakup. The rim breakup which leads to a bi-modal *pdf*(*d*) precludes this.
- Even if breakup is restricted to the sheet-thinning regime, the parameters in any universal *pdf*(*d*) will change with time because the experimental *pdf*(*d*) is doing so. This may make analytical forms for *pdf*(*d*) impossible to find.
- The ratio of MMD/D_{32} being approximately 1.2 is acceptable for sheet-thinning breakup, but not for bag breakup after the bag begins its collapse. In the latter case the ratio ranges from ~1 to ~1.7.
- These conclusions are also likely to apply if bag-and-stamen (multimode) breakup is occurring because of the presence of three disintegration processes—bag rupture and disintegration, rim collapse, and stamen breakup. This will lead to at least two distinct fragment size classes and perhaps a third.

Acknowledgements

This work was partially supported by the Weapons Systems Engineering Assessment Technology program, and the Laboratory Directed Research and Development program at Sandia National Laboratories which is a multiprogram laboratory operated by Sandia Corporation, a Lockheed Martin Company, for the United States Department of Energy's National Nuclear Security Administration under contract No. DE-AC04-94AL85000.

References

[1] Guildenbecher, D., López-Rivera, C., and Sojka, P., *Experiments in Fluids*, 46(3): 371-402, (2009).

[2] Guildenbecher, D.R., and Sojka, P.E., *ICLASS 2009: 11th International Conference on Liquid Atomization and Spray Systems*, 2009.

[3] Aalburg, C., van Leer, B., and Faeth, G.M., *AIAA Journal*, 41(12): 2371-2378, (2003).

[4] Hsiang, L.P., and Faeth, G.M., *International Journal of Multiphase Flow*, 21(4): 545-560, (1995).

[5] Hsiang, L.P., and Faeth, G.M., *International Journal of Multiphase Flow*, 18(5): 635-652, (1992).

[6] Faeth, G.M., Hsiang, L.P., and Wu, P.K., *International Journal of Multiphase Flow*, 21: 99-127, (1995).

[7] Chou, W.H., Hsiang, L.P., and Faeth, G.M., *International Journal of Multiphase Flow*, 23(4): 651-669, (1997).

[8] Chou, W.H., and Faeth, G.M., *International Journal of Multiphase Flow*, 24(6): 889-912, (1998).

[9] Liu, Z., and Reitz, R.D., *International Journal of Multiphase Flow*, 23(4): 631-650, (1997).

[10] Hwang, S.S., Liu, Z., and Reitz, R.D., *Atomization and Sprays*, 6(3): 353-376, (1996).

[11] Lee, C.S., and Reitz, R.D., *Atomization and Sprays*, 11(1): 1-19, (2001).

[12] Lee, C.H., and Reitz, R.D., *International Journal of Multiphase Flow*, 26(2): 229-244, (2000).

[13] Lee, C.H., and Reitz, R.D., *Atomization and Sprays*, 9(5): 497-517, (1999).

[14] Theofanous, T.G., Li, G.J., and Dinh, T.N., *Journal of Fluids Engineering*, 126(4): 516-527, (2004).

[15] Theofanous, T.G., Mitkin, V.V., Ng, C.L., Chang, C.-H., Deng, X., and Sushchikh, S., *Physics of Fluids*, 24(2): 022104, (2012).

[16] Theofanous, T.G., Mitkin, V.V., and Ng, C.L., *Physics of Fluids*, 25(3): 032101, (2013).

[17] O'Rourke, P.J., and Amsden, A.A., *International Fuels and Lubricants Meeting and Exposition*, 1987.

[18] Park, J.H., Yoon, Y., and Hwang, S.S., *Atomization and Sprays*, 12(4): 387-401, (2002).

[19] Taylor, G., *Proceedings of the Royal Society of London. Series A, Mathematical and Physical Sciences*, 201(1065): 192-196, (1950).

[20] Taylor, G.I., "The shape and acceleration of a drop in a high-speed air stream" in *The Scientific Papers of GI Taylor*, University Press, 1963.

[21] Lamb, H., *Hydrodynamics*, Cambridge University Press, 1916.

[22] Sellens, R., and Brzustowski, T., *Atomisation Spray Technology*, 1: 89-102, (1985).

[23] Xianguo, L.I., and Tankin, R.S., *Combustion Science and Technology*, 56(1-3): 65-76, (1987).

[24] van der Geld, C.W.M., and Vermeer, H., *International Journal of Multiphase Flow*, 20(2): 363-381, (1994).

[25] Cousin, J., Yoon, S.J., and Dumouchel, C., *Atomization and Sprays*, 6(5): 601-622, (1996).

[26] Dumouchel, C., *Particle & Particle Systems Characterization*, 23(6): 468-479, (2006).

[27] Lecompte, M., and Dumouchel, C., *Particle & Particle Systems Characterization*, 25(2): 154-167, (2008).

[28] Li, X., Li, M., and Fu, H., *Atomization and Sprays*, 15(3): 295-322, (2005).

[29] Dechelette, A., Babinsky, E., and Sojka, P., "Drop size distributions" in *Handbook of Atomization and Sprays*, Springer 2011.

[30] Masliyah, J.H., and Epstein, N., *Journal of Fluid Mechanics*, 44(03): 493-512, (1970).

[31] Han, J., and Tryggvason, G., *Physics of Fluids*, 11(12): 3650-3667, (1999).

[32] Han, J., and Tryggvason, G., *Physics of Fluids*, 13(6): 1554-1565, (2001).

[33] Tryggvason, G., Esmaeeli, A., Lu, J., and Biswas, S., *Fluid Dynamics Research*, 38(9): 660-681, (2006).

[34] Poon, E.K.W., Lou, J., Quan, S., and Ooi, A.S.H., *Physics of Fluids*, 24(8): 082107, (2012).

[35] Quan, S., Schmidt, D.P., Hua, J., and Lou, J., *Journal of Fluid Mechanics*, 640: 235-264, (2009).

[36] Quan, S.P., and Schmidt, D.P., *Physics of Fluids*, 18(10): 9, (2006).

[37] Wadhwa, A.R., Magi, V., and Abraham, J., *Physics of Fluids*, 19(11): 20, (2007).

[38] Wadhwa, A.R., Magi, V., and Abraham, J., *AIAA Journal*, 43(9): 1974-1983, (2005).

[39] Kékesi, T., Amberg, G., and Prahl Wittberg, L., *International Journal of Multiphase Flow*, 66(0): 1-10, (2014).

[40] Kulkarni, V., Guildenbecher, D.R., and Sojka, P.E., *ICLASS 2012, 12th International Conference on Liquid Atomization and Spray Systems*, 2012.

[41] Dai, Z., and Faeth, G.M., *International Journal of Multiphase Flow*, 27(2): 217-236, (2001).

[42] Hsiang, L.P., and Faeth, G.M., *International Journal of Multiphase Flow*, 19(5): 721-735, (1993).

[43] Gao, J., Guildenbecher, D.R., Reu, P.L., and Chen, J., *ILASS Americas 26th Annual Conference on Liquid Atomization and Spray Systems*, 2014.

[44] Gao, J., Guildenbecher, D.R., Reu, P.L., Kulkarni, V., Sojka, P.E., and Chen, J., *Optics Letters*, 38(11): 1893-1895, (2013).
[45] Gao, J., Guildenbecher, D.R., Reu, P.L., and Chen, J., *ILASS-Americas 25th Annual Conference on Liquid Atomization and Spray Systems*, 2013.
[46] Katz, J., and Sheng, J., *Annual Review of Fluid Mechanics*, 42: 531-555, (2010).
[47] Gao, J., Guildenbecher, D.R., Engvall, L., Reu, P.L., and Chen, J., *Applied Optics*, 53(27): G130-G138, (2014).
[48] Guildenbecher, D.R., Gao, J., Reu, P.L., and Chen, J., *Applied Optics*, 52(16): 3790-3801, (2013).
[49] Gao, J., Guildenbecher, D.R., Reu, P.L., and Chen, J., *Optics Express*, 21(22): 26432-26449, (2013).
[50] Tinevez, J.-Y., "Simple tracker," http://www.mathworks.com/matlabcentral/fileexchange/34040-simple-tracker, 2012.
[51] Guildenbecher, D.R., PhD Thesis, Purdue University, West Lafayette, Indiana, 2009.
[52] Flock, A.K., Guildenbecher, D.R., Chen, J., Sojka, P.E., and Bauer, H.J., *International Journal of Multiphase Flow*, 47(0): 37-49, (2012).
[53] Simmons, H.C., *Journal of Engineering for Power*: 315-319, (1977).